Atomistic Simulation of the Dissociative Adsorption of Water on Calcite Surfaces

Sebastien Kerisit,[†] Stephen C. Parker,*[,†] and John H. Harding[‡]

Department of Chemistry, University of Bath, Claverton Down, Bath, United Kingdom BA2 7AY, and Department of Physics and Astronomy, University College London, Gower Street, London, United Kingdom WC1E 6BT

Received: January 24, 2003; In Final Form: May 6, 2003

Atomistic simulation methods have been used to model the interaction of water with the $\{10\bar{1}4\}$ calcite surface and the energetics for the removal of carbonate groups in the presence of water. Electronic structure calculations show that associative adsorption of water is the energetically favored mode of adsorption on the $\{10\bar{1}4\}$ surface, that water is strongly bound to the surface, and that the atom-based simulations reproduce the energetics of adsorption. The use of atom-based molecular dynamics techniques on the calcite−water interface found that water loses its hydrogen-bond network when adsorbing on the surface and that it causes an oscillation of water density in the vicinity of the surface. Finally, we considered a possible reaction of the surface with water that would account for the presence of OH groups as observed experimentally on surfaces and would also constitute an initial step in the dissolution process. Our calculations suggest that carbonate groups at some step edges and low-index surfaces will dissociate water to form OH groups on the surface and release carbon dioxide but that this reaction does not take place on the undefective $\{10\bar{1}4\}$ surface.

Introduction

Calcite is a common mineral found in geological and biological systems. Therefore, an understanding of the structure and reactivity of calcite surfaces is important because it would allow us to gain insight into the dissolution and growth processes in both systems. As a consequence, calcite has been the subject of many experimental and simulation studies. For example, atomic force microscopy (AFM) has been used to study the $\{10\bar{1}4\}$ surface under aqueous conditions.[1] Reeder[2] studied the interaction of some divalent cations with the surface during growth by synchrotron X-ray fluorescence microanalysis. Jordan and Rammensee[3] used scanning force microscopy (SFM) to investigate the dissolution rate of the $\{10\bar{1}4\}$ surface. Stipp and Hochella[4] examined the {101} cleavage plane in ultrahigh vacuum by X-ray photoelectron spectroscopy (XPS) and low-energy electron diffraction (LEED). In earlier work, we used atomistic simulation techniques in order to investigate the structure and energy of calcite surfaces and model their interactions with water.[5,6] We have also considered the adsorption and segregation of cations at the surface[7] and the crystal dissolution from stepped surfaces.[8] Other groups employed similar methods to simulate bulk defects in calcite,[9] pit formation at the surface−water interface,[10] or the adsorption of water vapor[11] and liquids[12] on calcite. Comparatively few publications report quantum mechanical studies of calcite. Recent examples include work by Catti et al.,[13] who used periodic Hartree−Fock calculations to investigate the effect of pressure on the crystal structure, and Ruuska et al.,[14] who performed Hartree−Fock cluster calculations of water adsorption on the (001) surface.

One of the remaining questions we have begun to address is the role of water in the dissolution process. In our previous simulation studies, as indeed with other researchers, we assumed that water simply acts as a solvent, and yet the experimental observation of OH groups leads to a suggestion that water reacts with the calcite surfaces and dissociatively adsorbs. For example, Stipp and Hochella[4] found that when calcite was cleaved in air and then put into a UHV chamber, the surfaces showed no adsorption of water or carbon dioxide in XPS or TOF-SIMS (time-of-flight secondary ion mass spectroscopy). However, they did observe peaks corresponding to the presence of OH and H species on the surface. Hence they suggest that the water molecules are ejected from the surface in the UHV chamber, leaving only OH and H atoms strongly bonded to surface calcium atoms and carbonate groups, respectively. Infrared studies of the calcite−water interface also showed the presence of hydroxyl groups strongly bound to the surface.[15,16] Thus the aim of this work is to investigate the formation of OH species on calcite surfaces, which could also constitute an initial step in the dissolution process. We have initially focused on the $\{10\bar{1}4\}$ surface of calcite as it is now well established, both by experiment and by simulation, that it is the most stable surface and will dominate the morphology of most natural samples.

Theoretical Methods

In this study, we used both electronic structure calculations and atomistic simulations to investigate the interactions of water with the $\{10\bar{1}4\}$ surface of calcite. The aim of using the electronic structure calculations was to model associatively and dissociatively adsorbed water on the $\{10\bar{1}4\}$ surface, to identify which adsorption mode is energetically preferred, and to provide a test of the atomistic simulation approach. We calculated the electronic energies using the density functional theory (DFT) with the computer code VASP[17−20] (Vienna ab initio simulation package). This program follows the pseudopotential plane-wave approach where the valence electrons only are treated explicitly and the core electrons are replaced by ultrasoft Vanderbilt pseudopotentials.[21,22] The program employs the generalized gradient approximation (GGA) with the exchange-correlation

* To whom correspondence should be addressed: e-mail s.c.parker@bath.ac.uk.
[†] University of Bath.
[‡] University College London.

10.1021/jp034201b CCC: $25.00
Published on Web 07/04/2003

TABLE 1: Surface Energy Convergence as a Function of Slab Thickness

$CaCO_3$ layers	thickness (Å)	surface energy ($J \cdot m^{-2}$)
3	5.99	0.427
5	12.10	0.426
6	15.18	0.426

potential developed by Perdew et al.[23] The systems were relaxed by the conjugate-gradients method until the change in total energy was smaller than 10^{-5} eV. We used a $3 \times 3 \times 1$ Monkhorst−Pack K-mesh and a cutoff energy for the plane wave basis set of 500 eV. This approach has been used by others and us to successfully model mineral surfaces.[24,25] We also found that the surface energy of slabs consisting of five layers (i.e., 10 $CaCO_3$ units) separated by a 23 Å gap had converged for the $\{10\bar{1}4\}$ surface as shown in Table 1.

We also used two atomistic simulation techniques: molecular dynamics and energy minimization. We used the computer code DL_POLY[26] to perform molecular dynamics simulations of adsorption of water on the $\{10\bar{1}4\}$ surface primarily to investigate the effect of the dynamics on the structure and energetics. The systems were simulated in the NVE and NVT (constant number of particles, constant volume, and constant energy or temperature) and anisotropic NPT (constant number of particles, constant pressure, and constant temperature) ensembles by use of the Nosé−Hoover thermostat[27] and the Hoover barostat[27,28] with parameters for the relaxation time of 0.5 ps. The trajectories were generated by the Verlet leapfrog scheme using a time step of 0.2 fs. The Ewald summation method was used to calculate the electrostatic interactions.

Finally, we used the code METADISE,[29] which is designed to model dislocations, interfaces, and surfaces, to model the energetics of hydroxide formation on more complex calcite surfaces. In contrast to the previous techniques, this method assumes that the crystals are periodic in two dimensions. In addition, the atoms in the near surface region are allowed to relax mechanically, whereas those further away are held fixed at their bulk equilibrium positions.

The atomistic simulation techniques use interatomic potentials to describe the energy of a system in terms of atomic positions. They are based on the Born model of solids,[30] which separates the interactions between ions into long-range electrostatic forces and short-range interactions. The latter include a representation of the repulsion between the electron charge clouds, van der Waals attraction, and bond bending for the covalent carbonate anion. We included the shell model of Dick and Overhauser[31] to simulate ionic polarizability of the oxygen ions. In this model, the oxygen ion is represented as a core plus a shell coupled by a harmonic spring. The total charge is separated between the shell and the core. In the molecular dynamics simulations the shells were given a mass of 0.2 au.

The parameters we used for calcite were derived by Pavese et al.[32] in their study of the thermal dependence of structural and elastic properties of calcite. The intra- and intermolecular interactions of the water molecules were obtained from molecular dynamics simulations of liquid water as described in a previous paper on water adsorption on MgO surfaces.[33] The potential parameters for the interactions between water molecules and calcite surfaces are reported in a previous study on the water adsorption on calcite.[6] These parameters were also used to model the energetics of step growth[8] and later by Wright et al.,[34] albeit with a different calcite potential, to model the energetics of adsorption of water at the $\{10\bar{1}4\}$ surface of calcite. As noted in the Introduction, we wanted to model the interactions of the surface with hydroxyl groups. We used our previously reported strategy for deriving the potential model parameters.[7] These parameters have been previously employed for modeling portlandite [$Ca(OH)_2$]. We also added a repulsive potential between the carbon atom in the carbonate group and the oxygen of hydroxyl ions and water molecules to prevent unrealistic close contacts, particularly during MD simulations. The details of the potential parameters used to model hydroxyl ion can be found in Table 2. Table 3 compares the calculated and experimental[35] structural properties of calcium hydroxide.

TABLE 2: Potential Parameters Used to Model Hydroxyl Ion[a]

ion	charges: core	charges: shell	core−shell interaction (eV·Å)
hydroxyl oxygen (OH)	+0.80	−2.20	74.920 38
H	+0.40		

Buckingham potential[a]

ion pair (*ij*)	A_{ij} (eV)	ρ_{ij} (Å)	C_{ij} (eV·Å^6)
C−OH	761.0	0.3400	0.00
C−water oxygen (OW)	435.0	0.3400	0.00
Ca−OH	2170.0	0.2970	0.00
OH−carbonate O (OC)	16 372.0	0.2130	3.47
OH−OW	22 764.0	0.1490	14.47
OH−OH	22 764.0	0.1490	18.97
OH−water H (HW)	311.970	0.2500	0.00
OH−H	436.76	0.2500	2.50
OC−H	396.27	0.2300	0.00
OW−H	396.27	0.2500	10.00

Morse potential[b]

ion pair (*ij*)	D_{ij} (eV)	a_{ij} (Å^{-1})	r_0 (Å)
H−OH	7.0525	3.1749	0.942 85

[a] Buckingham potential form: $V_{ij} = A_{ij} \exp(-\rho_{ij}/r_{ij}) - C_{ij} r_{ij}^{-6}$ (short-range cutoff 20 Å). [b] Morse potential form: $V_{ij} = D_{ij}(1 - \exp[-\alpha_{ij}(r_{ij} - r_0)]^2 - D_{ij})$ (short-range cutoff 1.1 Å).

TABLE 3: Calculated and Experimental Structural Properties of Portlandite

	calcd	exptl[36]
a (Å)	3.658	3.589
c (Å)	4.793	4.911
a/*c*	0.763	0.731
volume (Å^3)	55.5	54.8
Ca−O (Å)	2.37	2.369
O−H (Å)	1.02	0.955
elastic constants (Gpa)		
C11	135.1	99.3
C12	45.6	36.2
C13	6.6	29.7
C33	26.0	32.6
C44	4.1	9.8
C66	44.7	31.6

The surface energies of the dry surfaces are given by

$$\gamma_{dry} = \frac{U_s - U_b}{A} \tag{1}$$

where U_s is the energy of the slab of crystal containing the surface, U_b is the energy of the bulk containing the same number of atoms, and A is the surface area. The surface energies of the hydrated surfaces for the associative adsorption of water are calculated as follows:

$$\gamma_{wet} = \frac{U_h - (U_b + nU_{H_2O})}{A} \tag{2}$$

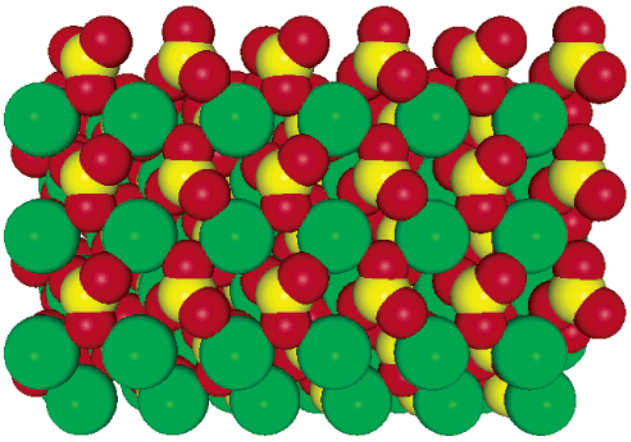

Figure 1. Plan view of the $\{10\bar{1}4\}$ surface (Ca = green, C = yellow, O = red).

where U_h is the energy of the hydrated surface, n is the number of water molecules, and U_{H_2O} is the energy of a liquid water molecule. We calculated the hydration energy of adsorption of water by comparing the energy of the pure surface and an isolated water molecule with the energy of a hydrated surface.

Results

We began by cleaving the crystal, exposing the $\{10\bar{1}4\}$ surface, and as noted previously,[5,6] revealing layers containing calcium atoms and carbonate groups. There are two equivalent carbonate groups with opposite orientations and they both have an oxygen atom in the plane of the layer, one above and one below as shown in Figure 1. We next compared the surface structure and energy using both electronic and atomistic simulation methods. We obtained a surface energy of 0.43 J·m^{-2} from the electronic structure calculation of the dry surface. The atomistic simulation gives a similar but slightly more positive surface energy of 0.59 J·m^{-2}. This is not surprising because the potential model lacks the full electronic relaxation available to an electronic structure calculation of a surface and hence an increase in surface energy is expected for potential model simulations. We then modeled a monolayer of water associatively adsorbed on the $\{10\bar{1}4\}$ surface. The water molecules are calculated to lie almost flat on the surface on a regular pattern in two opposite orientations, as has been suggested previously.[5] The oxygen atom of the water molecules is coordinated to surface calcium at a distance of 2.38 Å in the atomistic model and 2.37 Å in the electronic structure calculation. However, Hwang et al.[12] found, in their molecular dynamics calculation of water on the $\{10\bar{1}4\}$ surface, that the water molecules aligned with their hydrogen atoms pointing down, perhaps suggesting weak calcium−water binding. The two hydrogen atoms form hydrogen bonds to the two surface oxygen ions with carbonate oxygen−hydrogen distances of 1.68 and 2.01 Å in the atomistic simulation compared to 1.66 and 2.42 Å with the electronic method. The potential model gives a value for the hydration energy of −88.0 kJ·mol^{-1} and 0.21 J·m^{-2} for the surface energy. The energy of hydration calculated with VASP is −92.3 kJ·mol^{-1}, and the surface energy, 0.04 J·m^{-2}. This shows that our potential model can model reliably the adsorption of water on the $\{10\bar{1}4\}$ surface. Ruuska et al.[14] report an adsorption energy of −184.7 kJ·mol^{-1} for the interaction of water with a cluster model for the (001) surface. The difference in the magnitude of the interaction energy is not unexpected, as it has been shown experimentally that nanoparticles are more reactive and hence the magnitude of the adsorption energy increases.[36] We then dissociatively adsorbed a monolayer of water on the $\{10\bar{1}4\}$ surface. A hydroxyl group was positioned above each surface calcium atom and a hydrogen atom above a surface oxygen atom. On minimization the hydrogen atom moves from the surface oxygen to bond directly to the hydroxyl group oxygen atom, thereby re-forming a water molecule. This calculation suggests that, in contrast to the most logical interpretation of experimental observations, that dissociatively adsorbed water on calcite is energetically unfavorable on the $\{10\bar{1}4\}$ surface of calcite.

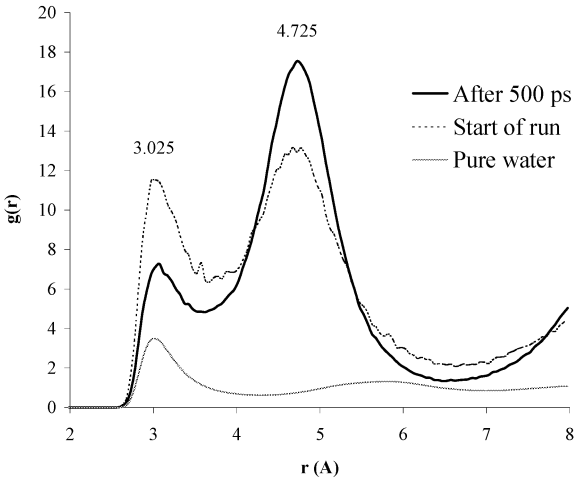

Figure 2. O_{water}–O_{water} radial distribution functions of water on the $\{10\bar{1}4\}$ surface and of water in a simulation of pure water.

Molecular Dynamics Simulations. As the electronic structure calculations suggested that water molecules prefer to adsorb associatively on the surface, we then investigated the effect of temperature and kinetics on the water−calcite interactions. We first considered a monolayer of water on the $\{10\bar{1}4\}$ surface and compared with the static calculations. The calcite slab consisted of 288 calcium carbonate units with a void of 30 Å separating two slabs. At the start of the simulation, the water molecules are positioned flat at 5.0 Å above the surface. The simulation was performed at 300 K and zero pressure. We equilibrated the system for 10 ps in the NVE ensemble and then for 10 ps in the NVT ensemble. The data were collected for 500 ps in the NVT ensemble.

The water oxygen−water oxygen radial distribution function, in Figure 2, shows two peaks. The first peak at 3.025 Å is the same peak as we find in the oxygen−oxygen radial distribution function of pure water, from a simulation of 256 water molecules in a cubic box. The second peak at 4.725 Å corresponds to the calcium−calcium distance. The dotted curve shows the radial distribution function after equilibration; some of the water molecules retain the water structure, indicated by the presence of the peak at 3.025 Å, whereas others are adsorbed on surface sites, as the peak at 4.725 Å suggests. The solid curve shows the radial distribution function after 500 ps. The first peak has diminished while the second peak has increased. This suggests that, due to the strong water−surface interaction, the water structure of hydrogen bonds is disrupted as the water molecules adsorb on the surface and, in addition, that there are two differently bonded water oxygen atoms, i.e., those that are strongly associatively bonded to surface calcium and those that are not (in contrast to hydroxyl and molecular water oxygen). The average calcium−water oxygen distance of 2.45 Å agrees with the experimental findings of Fenter et al.[37] Using high-resolution X-ray reflectivity, they found the presence of a monolayer of a hydroxyl species (either OH, OH_2, or OH_3) at

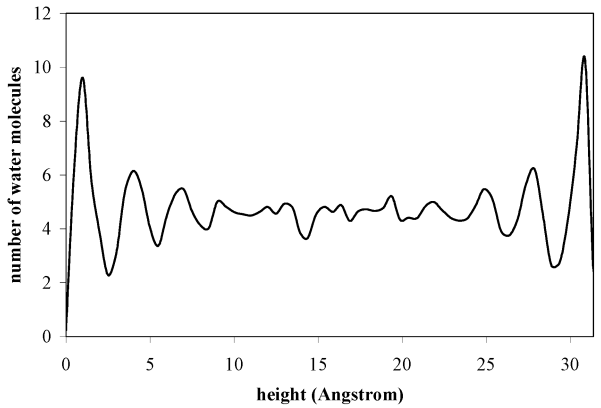

Figure 3. Average number of water molecules as a function of the position coordinate normal to the surface, where the two surfaces are at 0 and 32 Å.

2.50 ± 0.12 Å above the surface calcium ions. We obtained a value for the hydration energy of -69.5 kJ·mol^{-1}, which is about 20 kJ·mol^{-1} more positive than the hydration energy calculated from the static calculations. In the molecular dynamics simulation, the water molecules have kinetic energy and are not fixed at the lowest energy configuration; they will explore higher energy configurations. Thus the average hydration energy will always be higher than that obtained from energy minimization.

In a subsequent simulation, we filled the void between the slabs with water molecules and set the water density to the optimized density for this water potential at 300 K and zero pressure,[33] i.e., $\rho = 1.3$ g·cm^{-3}. The simulation was performed at 300 K for a simulation time of 500 ps in the NVT ensemble. Figure 3 is a histogram representing the average number of water molecules as a function of distance from the calcite slab. We can see from the simulation that the water density is greatest near the surfaces, and this has the effect of disrupting the bonding with the next layer of water and hence reducing the density of the next water layer. This causes an oscillation of water density away from the solid surface, which seems to be a common feature when water binds strongly to a mineral surface. Indeed, it has been seen both in theoretical studies, such as molecular dynamics simulations of MgO surfaces in liquid water,[33,38] and experimentally, for example, in a high-resolution X-ray reflectivity study[39] of mica surfaces in contact with water. Given the parallels in the results for water adsorption on the $\{10\bar{1}4\}$ surface of $CaCO_3$ and the (100) surface of MgO, i.e., similar structure and energies, it is worth noting that recent electronic structure simulations of water clusters on the (100) surface of MgO[40,41] showed that water dimerization can activate dissociation and leave OH groups on the surface. This still needs to be considered for calcite but is beyond our computer resource at present. However, a further mechanism we can investigate is the replacement of carbonate groups by hydroxyl ions, which is equivalent to dissociative adsorption of water accompanied by evolution of carbon dioxide. Another reason for considering this reaction is that it could potentially occur in samples exposed to air.

Reaction of Surface Carbonate Groups with Water. The dissociative adsorption of water and removal of carbon dioxide is likely to be site-specific. Therefore we considered a range of calcite surfaces. The surfaces chosen included the following five low-index surfaces: $\{10\bar{1}4\}$, $\{10\bar{1}0\}$, $\{0001\}$, $\{10\bar{1}1\}$, and $\{11\bar{2}0\}$ surfaces, which are often found in calcite samples. The $\{0001\}$ and $\{10\bar{1}1\}$ surfaces can be terminated in two different ways, either by a layer of calcium atoms or by carbonate groups.

TABLE 4: Surface and Hydration Energies of Calcite Surfaces

surface	γ_{dry} (J·m^{-2})	$\gamma_{hydrated}$ (J·m^{-2})	$E_{hydration}$ (kJ·mol^{-1})
$\{10\bar{1}4\}$	0.59	0.21	−88.0
$\{10\bar{1}0\}$	0.95	0.72	−99.8
$\{0001\}$ Ca	0.97	0.66	−81.0
$\{000\bar{1}\}$ CO_3	0.99	0.55	−96.7
$\{10\bar{1}1\}$ Ca	1.00	0.69	−97.0
$\{10\bar{1}1\}$ CO_3	1.14	0.82	−98.3
$\{11\bar{2}0\}$	1.39	0.59	−161.5
$\{10\bar{1}5\}$	0.67	0.62	−84.2
$\{10\bar{1}3\}$	0.75	0.65	−103.9
$\{31\bar{2}16\}$	0.70	0.61	−81.0
$\{31\bar{4}8\}$ (S)	0.95	0.67	−96.1
$\{31\bar{4}8\}$ (D)	0.82	0.64	−106.9

As $\{10\bar{1}4\}$ is the dominant surface, we also considered four vicinal surfaces: $\{10\bar{1}5\}$, $\{10\bar{1}3\}$, $\{31\bar{2}16\}$, and $\{31\bar{4}8\}$ surfaces, where each consists of $\{10\bar{1}4\}$ terraces and steps. In the case of the former two, the steps are dipolar, and in the latter two, the step edges are neutral. The $\{10\bar{1}3\}$ surface consists of $\{10\bar{1}4\}$ terraces that are offset from each other by one atomic layer down the $\{10\bar{1}1\}$ cleavage plane, whereas the $\{10\bar{1}5\}$ surface consists of $\{10\bar{1}4\}$ terraces offset by one atomic layer down the $\{0001\}$ surface. As the step edges are dipolar for these surfaces, they reconstruct forming an edge with 50% carbonate vacancies. The $\{31\bar{4}8\}$ surface consists of $\{10\bar{1}4\}$ planes and a monatomic step, which is a $\{10\bar{1}4\}$ plane too. The step is acute, which means that the angle between the lower terrace and the side of the step is 80° [exp. 78°].[42] The $\{31\bar{2}16\}$ surface again contains $\{10\bar{1}4\}$ terraces and a monatomic step, which is also a $\{10\bar{1}4\}$ plane but the angle is obtuse, i.e., the angle between the lower plane and the side of the step is 105° [exp. 102°].[42] The surfaces have all been described previously[5,6] and hence a detailed discussion of their structures is not necessary here. It is, however, worth noting that the $\{10\bar{1}0\}$ surface undergoes a large relaxation of the top layer and the surface carbonate groups tilt to form a faceted surface. Also the dry $\{11\bar{2}0\}$ surface, consisting of layers of both carbonate groups and calcium atoms, is the least likely, at least on energetics grounds, to occur in nature, as it has the highest surface energy of all the surfaces studied here. Finally, when we modeled the $\{31\bar{4}8\}$ surface using molecular dynamics, we found that the carbonate groups rotate to give a different configuration of the surface, which, when relaxed, has a lower surface energy. However, given the mobility of the carbonate groups, we expect both configurations are accessible; therefore both are considered. The configuration obtained from molecular dynamics will be noted D, and that from the static calculation, S. Table 4 gives the surface energy of the dry and hydrated surfaces as well as the energy of hydration.

Dry Surfaces. The reaction we chose to consider was

$$n\mathrm{CaCO_{3(surface)}} + \mathrm{Ca(OH)_{2(s)}} \rightarrow \mathrm{Ca}_n\mathrm{CO_{3(n-1)}(OH)_{2(surface)}} + \mathrm{CaCO_{3(s)}} \quad (3)$$

The first term represents the energy of a surface in a vacuum. The calculations were then repeated but with one CO_3^{2-} ion removed from the surface and replaced by two OH^- ions to give the hydroxylated surface. In each case, many different starting configurations were considered in order to find out the lowest energy adsorption site and to evaluate the spread of energies. When these energies were compared to the bulk calcite and calcium hydroxide lattice energies, -61.14 and -31.89 eV per calcium atom, respectively, the energy of reaction 3 for the different calcite surfaces could be calculated.

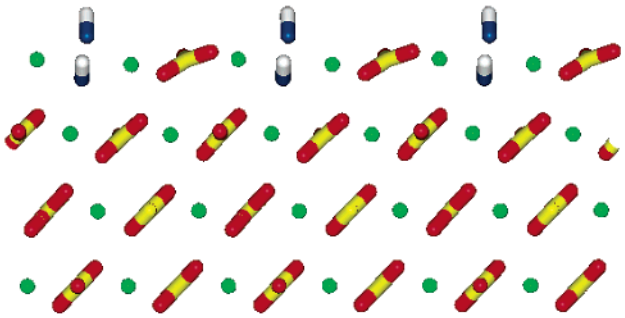

Figure 4. Dry {10$\bar{1}$4} surface after reaction with water (Ca = green, C = yellow, $O_{carbonate}$ = red, $O_{hydroxyl}$ = blue, H = white).

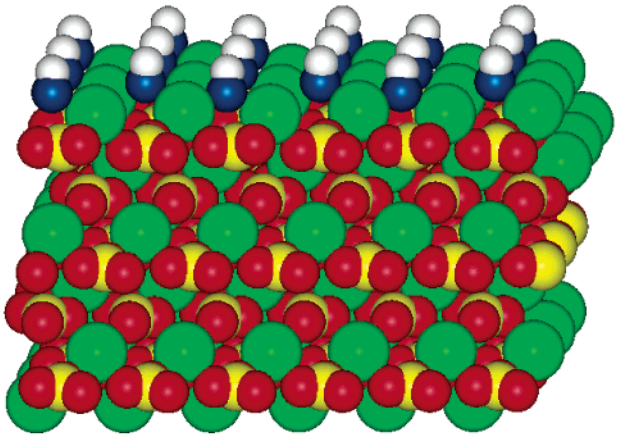

Figure 5. Dry {0001} carbonate terminated surface after reaction (Ca = green, C = yellow, $O_{carbonate}$ = red, $O_{hydroxyl}$ = blue, H = white).

The major difficulty with using atomistic simulations to model reactivity is that charges on the ions and the appropriate electron affinities need to be treated. The question of electron affinity could be ignored in reaction 3 because it has the same number of the two different charged oxygen atoms on each side of the equation.

Once the surfaces were modified, by removing carbonate ions and replacing them by hydroxyl groups, and allowed to relax to their minimum energy configuration, there was usually little relaxation of the crystal. This normally involved slight movement of the carbonate groups of the top layer. For example, in the case of the {10$\bar{1}$4} surface, the remaining half of the top carbonate groups rotate to lie almost flat on the surface as shown in Figure 4. The only exception is the {11$\bar{2}$0} surface, which undergoes large relaxation of the top three layers. On all the surfaces, the hydroxyl ions adsorb in the vacancy created by the dissolution of the carbonate group (see Figure 4). They are coordinated, through their oxygen atom, to two or sometimes three calcium atoms from the first two calcite layers. In the cases of the {0001} and {10$\bar{1}$1} carbonate-terminated surfaces, as the surface is terminated by half a layer of carbonate ions, once the remaining carbonate groups have been removed, the surface layer only consists of calcium atoms. The hydroxyl ions spread evenly on the surface and adsorb between two calcium atoms (see Figure 5), showing that it is energetically more favorable for the hydroxyl groups to coordinate to two calcium atoms rather than one. The situation is similar for the {10$\bar{1}$3} stepped surface, where the hydroxyl ions align along the step. The calcium−surface oxygen distances range from 2.21 to 2.50 Å when the hydroxyl ion is bonded to two calcium atoms and from 2.31 to 2.68 Å when it is bonded to three surface calcium atoms. The hydrogen atoms of the hydroxyl groups generally point away from the surface into the vacuum. In only three cases,

TABLE 5: Energy of Reaction 3 for Dry and Wet Calcite Surfaces and Standard Free Energy of Carbonate Removal

surface	ΔU_{solid} (kJ·mol^{-1}) of dry surfaces	ΔU_{solid} (kJ·mol^{-1}) of wet surfaces	$\Delta G°$ (kJ·mol^{-1}) of reaction 5
{10$\bar{1}$4}	14.7	18.9	100.3
{10$\bar{1}$0}	−37.4	−30.2	51.2
{0001} Ca	17.7	29.1	110.5
{0001} CO_3	11.4	38.7	120.1
{10$\bar{1}$1} Ca	−15.0	−4.0	77.4
{10$\bar{1}$1} CO_3	−108.7	−115.2	−33.8
{11$\bar{2}$0}	−161.7	−7.1	74.3
{10$\bar{1}$5}	6.0	−20.8	60.6
{10$\bar{1}$3}	−95.8	−72.3	9.1
{3$\bar{1}\bar{2}$16}	31.7	8.1	89.5
{31$\bar{4}$8} (S)	−78.9	−7.7	73.7
{31$\bar{4}$8} (D)	23.6	58.7	140.1

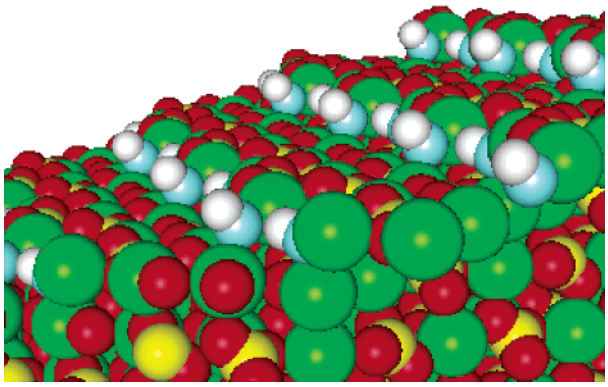

Figure 6. Dry {31$\bar{4}$8} surface after reaction with water (Ca = green, C = yellow, $O_{carbonate}$ = red, $O_{hydroxyl}$ = blue, H = white).

i.e., the {3$\bar{1}\bar{2}$16}, {10$\bar{1}$4}, and {10$\bar{1}$1} Ca surfaces, does a hydroxyl ion form a hydrogen bond with another hydroxyl ion, with distances of 1.92, 2.12, and 2.17 Å, respectively. There is no hydrogen bonding between hydrogen atoms and surface oxygens because the calcium−hydroxyl oxygen interaction is much stronger than the hydrogen−carbonate oxygen interaction.

Table 5 contains the energies of reaction of the dry surfaces. The most reactive low-index surfaces are the {10$\bar{1}$1} CO_3 and the {11$\bar{2}$0}, which are also the surfaces with the highest surface energy. Generally, the low-index surfaces that are open enough to allow hydroxyl groups to form short bonds are more stabilized. In contrast, of the stepped surfaces, the {10$\bar{1}$3} and {31$\bar{4}$8}(S) surfaces are most reactive. The reason is that for these the hydroxyl ions are able to form more short bonds with the surface when the shape of the step is acute (see Figure 6).

Hydrated Surfaces. Clearly an important component of the experimental system will be water. To reduce the level of complexity but still consider the potential disruption to the bonding between water and calcite, we modeled the effect of a monolayer of water initially on the pure and then on the reacted surfaces. We initially adsorbed a monolayer of water on the low-index surfaces of calcite and near the edges of the stepped surfaces. As above, we considered different geometries to locate the configuration of lowest energy. Table 4 lists the surface energy and hydration energy of the most stable geometry for the surfaces considered. As for the dry surfaces, we repeated the simulations but with one CO_3^{2-} ion removed from the top layer and replaced by two OH^- ions. When the hydrated surfaces are reacted, there is again little relaxation of the first carbonate layer. Indeed, for a number of surfaces, for example, the {10$\bar{1}$3} and {10$\bar{1}$5} surfaces, the carbonate ions of the first row of the upper terrace rotate back to an almost bulklike position. Only in the case of the {11$\bar{2}$0} surface do we observe a large

relaxation of the first three carbonate layers. Another general result is that, as observed for the dry surfaces, the hydroxyl ions tend to adsorb into the vacancy created by removing a carbonate group. The exceptions are for the carbonate-terminated polar surfaces (i.e., {0001} CO_3, {10$\bar{1}$1} CO_3, {10$\bar{1}$3}, and {10$\bar{1}$5}) where the hydroxyl groups form a hydroxide layer or cover the step edge. In each case, the hydroxyl ions are stabilized by coordinating to two or, occasionally, three calcium atoms from the first two surface layers. Bond distances to three calcium atoms are usually longer, between 2.32 and 2.72 Å, than bond distances to two calcium atoms, normally between 2.18 and 2.57 Å. On all the surfaces, the hydrogen atoms of the hydroxyl ions either point away from the surface or form a hydrogen bond with an oxygen atom of another hydroxyl ion, with bond distances ranging from 1.89 to 2.23 Å. On the {11$\bar{2}$0} surface only, a hydroxyl ion forms a hydrogen bond with a water molecule (with a bond distance of 1.71 Å). Water molecules are coordinated to one calcium atom with bond distances varying from 2.34 to 2.60 Å. In only one instance, the {31$\bar{4}$8} (S) surface, does a water molecule form two long bonds with calcium atoms: 2.69 and 2.70 Å. Water molecules very often form hydrogen bonds with surface oxygen, these bonds are normally short, between 1.53 and 1.96 Å, whereas hydrogen bonds to hydroxyl ions are less common and slightly longer, between 1.77 and 1.96 Å. The {0001} calcium-terminated surface is the only example of hydrogen bonding between water molecules, suggesting that, as for the pure surfaces, the water structure of hydrogen bonds is disrupted as the water molecules adsorb on the surface.

Table 5 lists the energy of reaction of the hydrated surfaces. The presence of water does not significantly modify the energy of reaction of the low-index surfaces and hence the relative order of reactivity is unaffected. A general observation is that the energy of reaction is more positive for dry surfaces because water stabilizes the stoichiometric surfaces more than the reacted surfaces. A probable cause is that in the reacted surfaces the hydroxyl groups adsorbed on the surface prevent the water molecules from forming the very stable surface layer described earlier.

Discussion

The reaction considered to date is that of a solid-state reaction; however, to compare directly with experiment we need to evaluate the free energy of reaction of the calcite surfaces with water including variation with pH and ion concentrations. A full treatment, including investigating the effect of pH and ionic strength, is beyond the scope of this paper. However, to give an indication of the free energies involved, we combined the solid-state reaction 3 with possible reaction 4 to give reaction 5. In this reaction the calcite surfaces react with a water molecule to hydroxylate the surface and release a carbon dioxide molecule, which is then hydrolyzed to a carbonic acid molecule by a second water molecule. The free energy of reaction 4 was obtained from experimental values.[43] All of the components of reaction 3 are solid; therefore, we can assume that the ΔU obtained from our calculations is similar to ΔG_{solid}^0. We added the experimental standard free energy of reaction 4 to our calculated energies to obtain the standard free energy of reaction 5:

$$CaCO_{3(s)} + 2H_2O_{(l)} \rightarrow Ca(OH)_{2(s)} + H_2CO_{3(aq)} \quad (4)$$

$$n\text{CaCO}_{3(\text{surface})} + 2H_2O_{(l)} \rightarrow \text{Ca}_n\text{CO}_{3(n-1)}(\text{OH})_{2(\text{surface})} + H_2CO_{3(aq)} \quad (5)$$

TABLE 6: Standard Free Energy of Removing Ions from Growth Steps[a]

		acute - dynamic	obtuse
mode 1	removal of $CaCO_3$	144.6	159.7
mode 2	carbonate removal	140.1	89.5
	calcium removal	4.5	70.2

[a] Energies are given in kilojoules per mole.

We only considered the hydrated calcite surfaces, as the surfaces will almost always be in contact with liquid or vapor water. The standard free energies of reaction 5 are given in Table 5.

Table 5 shows that all the standard free energies of reaction are endothermic except for the carbonate-terminated {10$\bar{1}$1} surface. The reaction is surface-specific and the free energies spread over about 175 kJ·mol^{-1}. As expected, the dominant {10$\bar{1}$4} surface is one of the most resistant surfaces and is not predicted to react to a large extent. The most reactive surfaces, namely, the {10$\bar{1}$3}, {10$\bar{1}$5}, {10$\bar{1}$0}, and carbonate-terminated {10$\bar{1}$1} surfaces, are either polar or faceted surfaces. Thus we predict that detailed analysis of the {10$\bar{1}$0} and particularly the {10$\bar{1}$1} surfaces will reveal them to have significant hydroxyl concentration. The stabilization of the two polar steps ({10$\bar{1}$3} and {10$\bar{1}$5} surfaces) could affect the morphology of stepped surface features such as etch pits and growth hillocks.

Finally, to begin to address whether removing first CO_3^{2-} and then Ca^{2+} from a step edge will be different from removing both together, we have calculated the free energy of forming a double kink site at the step edges of the {31$\bar{4}$8} and {3$\bar{1}\bar{2}$16} surfaces as in reaction 6. In a similar way as described above, we combined the energy of reaction 6 with the experimental free energy of reaction 7 to obtain an estimate of the free energy of reaction 8:

$$n\text{CaCO}_{3(\text{surface})} \rightarrow (n-1)\text{CaCO}_{3(\text{surface})} + \text{CaCO}_{3(s)} \quad (6)$$

$$\text{CaCO}_{3(s)} \rightarrow \text{Ca}^{2+}{}_{(aq)} + \text{CO}_3{}^{2-}{}_{(aq)} \quad (7)$$

$$n\text{CaCO}_{3(\text{surface})} \rightarrow (n-1)\text{CaCO}_{3(\text{surface})} + \text{Ca}^{2+}{}_{(aq)} + \text{CO}_3{}^{2-}{}_{(aq)} \quad (8)$$

In Table 6, we give the standard free energy of removing ions from the growth steps. Mode 1 refers to removal of both Ca^{2+} and CO_3^{2-} together. It costs 15 kJ·mol^{-1} more to form a double kink site at the obtuse than at the acute step edge. If this free energy is closely related to the activation free energy, then we would predict the obtuse step to be the slow-dissolving step in a one-step dissolution reaction. Although the obtuse step edge is seen experimentally to be the fast-dissolving step.[42,44] We next considered a possible two-step pathway, mode 2, whereby the step edges react first following reaction 3 and then lose to the solution a calcium atom and the two hydroxyl ions just formed. The hydroxyl ions will subsequently react with the bicarbonate molecule formed in reaction 5 to give water and carbonate ion, therefore completing the thermodynamic cycle.

Table 6 shows that the effective activation free energy of the obtuse step is reduced to 90 kJ·mol^{-1}, whereas the acute is unchanged. This causes the effective energy of dissolution of the obtuse step to become lower than that of the acute step, which could account for experimental observations. These calculations suggest that the dissolution process may be more complex than simply removing one calcium carbonate unit at a time and that intermediate states might be involved and modify the dissolution by reducing the effective energy of dissolution. Therefore, we need to take into account other possible dissolu-

tion pathways in our calculations, and we will thus investigate next a similar reaction whereby a calcium ion is removed from the surface and bicarbonate molecules are formed.

Conclusion

We employed electronic and atomistic simulation methods to investigate the interactions of water with the {10$\bar{1}$4} surface of calcite and the reaction of water with low-index and stepped surfaces that would dissociate water and remove a carbonate group from the surface.

We found, using electronic structure calculations, that water prefers to adsorb associatively on the {10$\bar{1}$4} surface and that our potential model successfully reproduces the structure and energy of the adsorption of water on the {10$\bar{1}$4} surface.

Molecular dynamics simulations of water on the {10$\bar{1}$4} showed that the strong water−surface interactions break the water hydrogen-bond network of the first monolayer, resulting in an oscillation of the water density in the vicinity of the surface.

Finally, we performed extensive energy minimization calculations on several calcite surfaces and found that the reaction of water with surface carbonate groups could be a first step in the dissolution process and would occur at step edges and defective surfaces rather than at the perfectly flat {10$\bar{1}$4} surface.

In the future, we intend to use a combination of potential-based and ab initio molecular dynamics to investigate whether intermolecular water interactions could induce water dissociation at the surface, as it has been shown for the (100) MgO surface,[40,41] and the effect of varying the composition of solution and surface on the surface behavior.

Acknowledgment. We thank EPSRC, Grant GR/H0185, and JREI, Award JR99BAPAEQ, for financial support.

References and Notes

(1) Liang, Y.; Lea, A. S.; Baer, D. R.; Engelhard, M. H. *Surf. Sci.* **1996**, *351*, 172.
(2) Reeder, R. J. *Geochim. Cosmochim. Acta* **1996**, *60*, 1543.
(3) Jordan, G.; Rammensee, W. *Geochim. Cosmochim. Acta* **1998**, *62*, 941.
(4) Stipp, S. L.; Hochella, M. F. *Geochim. Cosmochim. Acta* **1991**, *55*, 1723.
(5) de Leeuw, N. H.; Parker, S. C. *J. Chem. Soc., Faraday Trans.* **1997**, *93*, 467.
(6) de Leeuw, N. H.; Parker, S. C. *J. Phys. Chem. B* **1998**, *102*, 2914.
(7) de Leeuw, N. H.; Parker, S. C. *J. Chem. Phys.* **2000**, *112*, 4326.
(8) de Leeuw, N. H.; Parker, S. C.; Harding, J. H. *Phys. Rev. B* **1999**, *60*, 13792.
(9) Fisler, D. K.; Gale, J. D.; Cygan, R. T. *Am. Mineral.* **2000**, *85*, 217.
(10) McCoy, J. M.; LaFemina, J. P. *Surf. Sci.* **1997**, *373*, 288.
(11) Stöckelmann, E.; Hentschke, R. *Langmuir* **1999**, *15*, 5141.
(12) Hwang, S.; Blanco, M.; Goddard, W. A., III *J. Phys. Chem. B* **2001**, *105*, 10746.
(13) Catti, M.; Pavese, A.; Aprà, E.; Roetti, C. *Phys. Chem. Miner.* **1993**, *20*, 104.
(14) Ruuska, H.; Hirva, P.; Pakkanen, T. A. *J. Phys. Chem. B* **1999**, *103*, 6734.
(15) Kuriyavar, S. I.; Vetrivel, R.; Hedge, S. G.; Ramaswany, A. R.; Chakrabarty, D.; Mahapatra, S. *J. Mater. Chem.* **2000**, *10*, 1835.
(16) Neagle, W.; Rochester, C. H. *J. Chem. Soc., Faraday Trans.* **1990**, *86*, 181.
(17) Kresse, G.; Hafner, J. *Phys. Rev. B* **1993**, *47*, 558.
(18) Kresse, G.; Hafner, J. *Phys. Rev. B* **1994**, *49*, 14251.
(19) Kresse, G.; Furthmuller, J. *Comput. Mater. Sci.* **1996**, *6*, 15.
(20) Kresse, G.; Furthmuller, J. *Phys. Rev. B* **1996**, *54*, 11169.
(21) Vanderbilt, D. *Phys. Rev. B* **1990**, *41*, 7892.
(22) Kresse, G.; Hafner, J. *J. Phys.: Condens. Matter* **1994**, *6*, 8245.
(23) Perdew, J. P.; Chevary, J. A.; Vosko, S. H.; Jackson, K. A.; Pederson, M. R.; Singh, D. J.; Fiolhas, C. *Phys. Rev. B* **1992**, *46*, 6671.
(24) de Leeuw, N. H.; Purton, J. A. *Phys. Rev. B* **2001**, *63*, 195417.
(25) de Leeuw, N. H.; Purton, J. A.; Parker, S. C.; Watson, G. W.; Kresse, G. *Surf. Sci.* **2000**, *452*, 9.
(26) Forester, T. R.; Smith, W. DL_POLY *user manual*; CCLRC, Daresbury Laboratory: Daresbury, Warrington, U.K., 1995.
(27) Hoover, W. G. *Phys. Rev. A* **1985**, *31*, 1695.
(28) Melchionna, S.; Ciccotti, G.; Holian, B. L. *Mol. Phys.* **1993**, *78*, 533.
(29) Watson, G. W.; Kelsey, E. T.; de Leeuw, N. H.; Harris, D. J.; Parker, S. C. *J. Chem. Soc., Faraday Trans.* **1996**, *92*, 433.
(30) Born, M.; Huang, K. *Dynamical Theory of Crystal Lattices*; Oxford University Press: Oxford, U.K., 1954.
(31) Dick, B. G.; Overhauser, A. W. *Phys. Rev.* **1958**, *112*, 90.
(32) Pavese, A.; Catti, M.; Parker, S. C.; Wall, A. *Phys. Chem. Miner.* **1996**, *23*, 89.
(33) de Leeuw, N. H.; Parker, S. C. *J. Phys. Chem. B* **1998**, *58*, 13901.
(34) Wright, K.; Cygan, R. T.; Slater, B. *Phys. Chem. Chem. Phys.* **2001**, *3*, 839.
(35) Desgranges, L.; Grebille, D.; Calvarin, G.; Chevrier, G.; Floquet, N.; Niepce, J. C. *Acta Crystallogr. B* **1993**, *49*, 812.
(36) Stark, J. V.; Park, D. G.; Lagadic, I.; Klabunde, K. J. *Chem. Mater.* **1996**, *8*, 1904.
(37) Fenter, P.; Geissbulher, P.; DiMasi, G. *Geochim. Cosmochim. Acta* **2000**, *64*, 1221.
(38) McCarthy, M. I.; Schenter, G. K.; Scamehorn, C. A.; Nicholas, J. B. *J. Phys. Chem.* **1996**, *100*, 16989.
(39) Cheng, L.; Fenter, P.; Nagy, K. L.; Schlegel, M. L.; Sturchio, N. C. *Phys. Rev. Lett.* **2001**, *87*, 156103.
(40) Giordano, L.; Goniakowski, J.; Suzanne, J. *Phys. Rev. Lett.* **1998**, *81*, 1271.
(41) Odelius, M. *Phys. Rev. Lett.* **1999**, *82*, 3919.
(42) Park, N.-S.; Kim, M.-W.; Langford, S. C.; Dickinson, J. T. *J. Appl. Phys.* **1996**, *80*, 2680.
(43) Johnson, D. A. *Some Thermodynamic Aspects of Inorganic Chemistry*, 2nd ed.; University Press: Cambridge, U.K., 1982.
(44) Liang, Y.; Baer, D. R. *Surf. Sci.* **1997**, *373*, 275.